# Excitation of Plasma Modes by Electron Beams

Claudio Elias da Silva –C.E.da Silva[1], Altair Souza de Assis –A.S.de Assis[2],
Alan Freitas Machado – A.F.Machado[3]

[1](Quantum Electronics/Physics Institute - UERJ, RJ-Brazil)
[2](Mathematics Institute/UFF, Niteroi-Brazil)
[3](Theoretical Physics/ Physics Institute - UERJ, RJ-Brazil)
*Corresponding Author: Claudio Elias da Silva –C.E.da Silva*

***Abstrac:****We present in this paper a numerical study of the excitation of high and low frequency waves – electromagnetic and electrostatic – by the electron beams. This study is useful for fusion plasma physics as well as for auroral plasma physics. We have solved the fully kinetic plasma dispersion relation using the numerical code developed by A. F. Viñas at NASA/GSFC, and found the real frequency and the growth/damping rate for the problem relevant to the plasma modes. Those modes are the electromagnetic/electrostatic ion cyclotron wave (EMIC/EIC), the kinetic Alfvén wave (KAW), the fast magnetosonic wave (FMW), the ion and electron whistler (IW/EW) waves, lower/upper hybrid (LHW/UHW) waves. In all the cases, as a suitable example, the source of free energy are electron beams, propagating parallel to the geomagnetic field, in the so called inverted-V events, which are direct associated with auroras. We present some features of the growth/damping rate for the various modes, in situations where the target plasma parameters are changed; such as, the background electrons and ions temperature, density, and the electron beam density and drift velocity as well. The obtained results can be used, for instance, in a test-particle simulation code, to investigate the electron and ion acceleration in auroral plasma region, by wave–particle interaction. The target plasma region, by wave–particle interaction. The target plasma data used are the ones from the DE 1 satellite.*

***Keywords:****Dielectric Tensor, Eigenfrequency, Cherenkov Damping, Kinetic Alfven Wave, Fast Magnetosonic Wave, Electromagnetic Ion Cyclotron Wave, Electrostatic Ion Cyclotron Wave, Whistler Wave, Lower Hybrid Wave, Upper Hybrid Wave*

## I.    Introduction

The presence of wave instabilities in a plasma medium has been under consideration for decades [Parks 1991]. Waves in Plasma is one of the many electrodynamic phenomena occurring in space and surely one of the most important. A broad range of waves frequencies have been detected in space [Persoon, 1988; Wang, 1996]. Different sources as, solar wind, magnetosphere, and ionosphere and so on, can be the origin of disturbances that generate wave excitation in space. In spite of plasma waves being intensively studied, there are yet many questions to be answered about the source of energy, propagation and polarization properties and many phenomena associated with the appearance of instabilities. For instance, Temerin and Lysak [1984] studied excitation of low-frequency EMIC waves by inverted-V electron beams, assuming a cold plasma dispersion, while Lin et al. [1989] included kinetic effects. We have also considered full kinetic effects, but we included besides low-frequency, electromagnetic and electrostatic high-frequency modes in the analysis of wave instabilities, since the auroral background plasma is susceptible to different variations due to dynamics processes such as magnetic storms and substorms, and therefore can support several different modes via the same source. These modifications in the plasma create great and fast changes inside the bulk of the magnetosphere. Auroral region is strongly affected by these disturbances and even satellites cannot describe efficiently all kinds of variations, and relate them with the different responses provided during these events. In trying to describe the different conditions of the auroral region, mainly during the presence of dynamic processes that produce large disturbances, we have employed simulated data through the variation of beam and plasma background parameters, which are of relevant importance to study and understand the appearance of plasma wave instabilities.

The physical parameters that we have changed by simulation method are very important to describe the medium behavior. Background plasma temperature and density, beam energy and direction of wave propagation relative to the magnetic field are some of these parameters. The reason for choosing these parameters in the

analysis is related to the satellite measurements in its pass through auroral region, and in particular, the data from distribution function analysis give us important information on the auroral environment behavior. On the other hand, simulating new values from these physical parameters, we are able to investigate more properly, in what different conditions the wave modes can be excited.

Our purpose in this paper, therefore, is to analyze the appearance of wave instabilities in the auroral region, when the plasma medium is excited by energetic electron beams propagating parallel to the magnetic field, in the inverted-V structure, as can be seen in the Figure, as a source of free energy. We have developed a numerical code, using simulation method to solve the dispersion equation able to describe the linear wave plasma behavior under target plasma changes.

The region in focus extends around 2000 – 7000km altitude, where the background plasma data used in our paper is in agreement with the observations of the DE 1 satellite. Many of the instruments on the DE 1 satellite have the capability to cover relatively wide ranges of frequencies with high spectral resolution [Peterson et al. 1988]. The solar wind and the ionosphere can be considered the main source of magnetospheric plasma. It was Shelley et al. [1972], which reported during a magnetic storm a large presence of O+ in the energetic ion flux inside the magnetosphere. He also reported the large ratio O+/H+ observed from the ionosphere, compared with the same ratio in the solar wind, suggesting the ionosphere as being the source, which was afterwards confirmed by the S3-3 satellite [Sharp et al., 1977]. The DE 1 satellite has also observed the presence of O+ and H+ in the auroral region, which concentration varies with height. Below 5000 km the concentration suggested is about 90% of O+ and 10% of H+, besides smaller percentages of other ion species [Yau and Whalen, 1993]. On the other hand, Lin et al. [1989] has suggested 90% of H+ and 10% of O+ above 2000km altitude. We have considered different possibilities in the analysis of instabilities, including the variation of ions concentration in the range analyzed.

The composition and energy involved in the plasma under study, is in agreement with Lin et al., [1989]. Therefore, our background plasma is composed of cold electrons. A very low density has been considered in the auroral plasma which total electron density is about 4cm$^{-3}$ and the temperature varying in the range of 1 to 100 eV. An energetic electron beam with temperature around 5keV and energy of about 10keV, as can be seen in the Figure 1, while the only positive ion species considered are hydrogen and oxygen, as the main species, since the minor ones, as N++, N+, He+ and O++ are neglected [see Wolf et al., 1986]. Due to the dynamics of the auroral region, the concentration of these species can change considerably with height, affecting the growth rate of some particular excited mode, characterizing the altitude dependence of some modes. This analysis is just possible by using again simulation process. Since our purpose here is to analyze and understand in which different conditions instabilities can be generated, we simulate some auroral conditions, as we have mentioned before, to observe the growth of each mode.

The numerical codes that we use in this work are suitable to study electromagnetic and electrostatic linear plasma wave instabilities. The codes and their subroutines, solve the Vlasov dispersions equation for a distribution function that has a temperature anisotropy in the various species and a drift velocity parallel to the background magnetic field in this code, in the z-axis and the wave number k is in the (x, z)plane. The dispersion relation for oblique propagation it is solved numerically using the Müller method (ZANLYT routine) to obtain the roots of the dispersion relation. The program it was written in Fortran 77.

The numerical code used reproduces the results of WHAMP and Miller and Viñas [1993] have used it successfully. In addition, our results for electromagnetic low-frequency instabilities are in agreement with the results of Lin et al. [1989]. However, for the high frequency modes some novel features are present. In addition, still in the low frequency range, for the KAW, we have some new results. For the low frequency fast magnetosonic, no conclusive behavior is it shown. On the other hand, it is clear that in the range of auroral plasma parameter variations, EMIC, KA and LH can growing a reasonable rate, FM and IW can grow slowly and EW does not grow at all. Note that the code are suitable to study the upper hybrid, electron cyclotron (Bernstein), and EIC waves but we leave the results for a future paper.

This paper is it organized as follows. In chapter 2, we present the general dispersion relation for the auroral plasma modes. In chapter 3, we present the analysis of different modes propagating in the auroral region excited by energetic electron beams. In chapter 4, we present the plots as a numerical result of the dielectric tensor elements. Finally, in chapter 5, we present the conclusions.

## II.     Dispersion Relation

To study the plasma dispersion relation, we consider the auroral background plasma to be maxwellian and collisionless, composed by electrons, O$^{+}$, H$^{+}$ and an energetic electron beam crossing the auroral background plasma, parallel to the geomagnetic field. The equilibrium distribution function is then,

$$f_i = n_i \left(\frac{m}{2\pi T_i}\right)^{3/2} \exp\{-m\,[(v_\parallel - u_i)^2 + v_\perp{}^2]/2T_i\} \tag{1}$$

Where $n_i$, $T_i$ and $u_i$ are the number density, temperature and drift velocity of the ithcomponent. Therefore, the dielectric tensor elements, obtained from the standard linear analysis of the Maxwell-Vlasov equations for a magnetized plasma, can be found in the textbooks, such as Melrose[1980] and Stix [1992]. In spite of it, we present the tensor elements as follow,

$$\varepsilon_{xx} = \sum_s \frac{\omega_{ps}^2}{\omega^2}(\mu_s - 1) + \sum_s \sum_{-\ell}^{+\ell} \frac{\omega_{ps}^2}{\omega^2} \frac{\ell^2 \Lambda_l(\lambda_s)}{\lambda_s} \mu_s \bar{\xi}_s Z(\xi_s) \tag{2}$$

$$\varepsilon_{xy} = i \sum_s \sum_{-\ell}^{+\ell} \frac{\omega_{ps}^2}{\omega^2} \ell \Lambda_\ell^{'}(\lambda_s) \mu_s \bar{\xi}_s Z(\xi_s)$$

$$\varepsilon_{xz} = \sum_s \frac{\omega_{ps}^2}{\omega^2} \frac{K_\perp}{K_\parallel}(1 - \mu_s) + 2\sum_s \sum_{-\ell}^{+\ell} \frac{\omega_{ps}^2}{\omega^2} \frac{\ell \Lambda_\ell \Omega_s}{K_\perp \alpha_{\parallel s}} Y_s \bar{\xi}_s Z(\xi_s)$$

$$\varepsilon_{yx} = -\varepsilon_{xy}$$

$$\varepsilon_{yy} = \sum_s \frac{\omega_{ps}^2}{\omega^2}(\mu_s - 1) + \sum_s \sum_{-\ell}^{+\ell} \frac{\omega_{ps}^2}{\omega^2}\left(\frac{\ell^2 \Lambda_\ell}{\lambda_s} - 2\lambda_s \Lambda_\ell^{'}\right)\mu_s \bar{\xi}_s Z(\xi_s)$$

$$\varepsilon_{yz} = -2i \sum_s \sum_{-\ell}^{+\ell} \frac{\omega_{ps}^2}{\omega^2} \frac{\lambda_s \Omega_s \Lambda_\ell^{'}}{K_\perp \alpha_{\parallel s}} Y_s \bar{\xi}_s Z(\xi_s)$$

$$\varepsilon_{zx} = \varepsilon_{xz}$$
$$\varepsilon_{zy} = -\varepsilon_{yz}$$

$$\varepsilon_{zz} = 2\sum_s \frac{\omega_{ps}^2}{\omega^2}\left[\left(\frac{\omega}{K_\parallel \alpha_{\parallel s}}\right)^2 + \frac{1}{2}(\mu_s - 1)\frac{K_\perp^2}{K_\parallel^2}\right] + 2\sum_s \sum_{-\ell}^{+\ell} \frac{\omega_{ps}^2}{\omega^2} \Lambda_s Y_s^{\ 2} \bar{\xi}_s Z(\xi_s)$$

Where,

$$\bar{\xi}_s = \frac{\omega - K_\parallel u_{\parallel s} - (1 - \mu_s^{-1})\ell\Omega_s}{K_\parallel \alpha_{\parallel s}}$$

$$\xi_s = \frac{\omega - K_\parallel u_{\parallel s} - \ell\Omega_s}{K_\parallel \alpha_{\parallel s}}$$

$$\Lambda_\ell(\lambda_s) = \exp(-\lambda_s)I_\ell(\lambda_s)$$

$$Y_s = \frac{\omega - \ell\Omega_s}{K_\parallel \alpha_{\parallel s}}$$

$$\mu_s = \frac{\alpha_{\perp s}^2}{\alpha_{\parallel s}^2}$$

With,

$$\omega_{ps}^2 = \frac{4\pi n_s q_s^2}{m_s}$$

the index s means particles species (ions and electrons), while $\ell$ is an integer number meaning the cyclotron harmonic number.

In the above, $\Omega_s = q_s B_0/m_s$ cis the gyrofrequency for each species,$\alpha_{\perp s}^2 = 2KT_{\perp s}/m_s$ and $\alpha_{\parallel s}^2 = 2KT_{\parallel s}/m_s$ are the perpendicular and parallel thermal speeds for each species, respectively, $I_\ell(\lambda_s)$ is the modified Bessel function and,

$$Z(\xi_s) = \frac{1}{\pi^{1/2}} \int_{-\infty}^{+\infty} dx \frac{\exp(-x^2)}{x - \xi_s}, \ Im\xi > 0,$$

is the well-known plasma dispersion function [Stix, 1992].

The dielectric tensor presented above is generic and for this reason is extended for being used in both circumstances, magnetized and unmagnetized codes. The code is classified as magnetized whenever electrons and background protons are magnetized, but any other ion species are assumed for being unmagnetized. While in the unmagnetized code, electrons are the only magnetized species, all the ions are treated as unmagnetized.

We have developed a specie code to treat more properly the unmagnetized lower hybrid wave, to save computation time. The unmagnetized electrostatic dielectric tensor can be shown in terms of its general expression as:

$$\varepsilon(\vec{K}, \omega) = (1 - \sum_s \frac{\omega_{pi}}{\omega^2})\vec{I} - \sum_s \frac{\omega_{ps}^2}{\omega^2} \int \frac{\vec{v}\vec{v}(\vec{K} \cdot (\partial f_{s0})/(\partial \vec{v}))}{(\vec{K} \cdot \vec{v} - \omega)} d^3\vec{v} \tag{3}$$

where the wave vector $\vec{K} = (k_x, 0, k_z)$ and the second somatory is relative to the ion species only, while the effective distribution function shows the form,

$$f_{s0}(v_x, v_y, v_z) = \frac{1}{\pi^{3/2}\alpha_{\perp s}^2 \alpha_{\parallel}} \exp\left\{-\left[(v_x - u_x)^2/\alpha_{\perp}^2 + (v_y - u_y)^2/\alpha_{\perp}^2 + (v_z - u_z)^2/\alpha_{\parallel}^2\right]\right\} \tag{4}$$

where, $u_x$, $u_y$, and $u_z$ are the drift velocities.

In this analysis, we have solved numerically the fully dispersion relation for plasma waves excited by electron beams. Finally, the general plasma wave dispersion relation presents the form,

$$\det[D_{ij}(\vec{K}, \omega)] = \det\left[\frac{c^2}{\omega^2}(K_j K_j - K^2\delta_{ij}) + \varepsilon_{ij}\right] = 0 \tag{5}$$

where, $\delta_{ij}$ is the delta of Kronecker and $\varepsilon_{ij}$ is given by Eq.2 as a generic case and by Eq.3 only for electrostatic waves.

## III.    Wave Propagation Analysis

In this section, we present plots showing the growth of the wave instabilities or damping corresponding to the numerical solution of Eq.5, considering the auroral plasma medium as seen by the DE 1 satellite measurements on the auroral pass of day 318, 1981, reported by Winninghan and Burch [1984]. All the parameters used here are in agreement with the electron distribution function model presented by Lin et al. [1989]. We have considered the region extending from $2000 - 7000$ km altitude, where the dominant species are hydrogen and oxygen ions and we evaluate how the concentration from these species with height can affect the growth rate modes.

Although we are assuming, at first, hydrogen ions as the dominant species at high altitude and the composition of 90% of $H^+$ and 10% of $O^+$, we have also studied the composition of 10% of $H^+$ and 90% of $O^+$ in lower and mid altitude where the oxygen is the dominant specie. Just for comparison to show that, some modes can be excited in both conditions and that growth rates extend in a broad range inside the background plasma environment.

The Figure 2 shows the real frequency $\omega$ and the growth rate $\gamma$ to the EMIC mode, both normalized to the proton plasma frequency, $\omega_p$, in a quasi-perpendicular propagation $\theta = 89°$, while the wave number is multiplied by $c/\Omega_p$. The data corresponding to the background plasma are in agreement with Lina et al. [1989]. From the figure, we may observe a broad wave number spectrum associate with the growth. The real frequency corresponding to the maximum growth is about $0.4\Omega_p$, what means, below the proton cyclotron frequency ($\Omega_p$), characterizing a range of low frequency propagation. This growth rates tend to decrease whenever $\theta \to 0°$.

The Figure 3, shows the same mode, but normalized to the proton cyclotron frequency. The frequency corresponding to the maximum growth is about $0.5\Omega_p$ and still below the proton cyclotron frequency, for the same background plasma conditions as seen before.

In the Figure 4, it is still possible to observe the wave propagation and the growth, but in a narrow wave number range, when the background plasma temperature increases from 15eV to 100eV. In this temperature, the plasma can still be considered as cold.

In the background plasma parameters, the ratio between drift to the thermal beam velocity is about 1.4. Whenever we want to change the beam energy to analyze the appearance of instabilities, we vary this ratio. The Figure 5 shows the presence of instabilities in the plasma, when the ratio reaches 3, what means a relativistic beam energy, since we are considering the same beam temperature. Above this ratio, the hydrogen EMIC wave is found to be weakly unstable. On the other hand, taking off the beam, no instability is found, as it should be.

The numerical simulation, enable us to many other variations with the plasma parameters in the sense of analyzing the propagation of each mode, its growth or damping in accordance with energy transference between waves and background plasma particles. To conclude the observations relative to the hydrogen EMIC mode, we are just going to comment some new results. For instance, we also observed the presence of growth when we changed the concentration of density between background and beam electrons, from 12% (standard value) to 40% of the beam density. Similar variation was done to the ions concentration and, we observed the presence of the growth until the oxygen concentration reaches 40% of the total ion density, but no more. Therefore, the hydrogen EMIC instabilities are driven by the inverted-V electron beam structure under different conditions. Our results for the EMIC modes are in agreement with Lin et al [1989].

The next step is to analyze the KA mode. The Figure 6 shows the plot ω, γ × θ for a fix k (k= 0.3) and θ varying from 1º to 89º. The wave growth is relevant in a broad range, and drops slowly with θ, but suffers a big fall when the angle reaches 87º. From the program output results it is possible to observe that the mode has, a left-hand polarization along its propagation, but it changes to the right-hand at θ = 87º (suggesting some kind of mode conversion) and turns again to the left-hand polarization until 89º. The maximum growth occurs at ω = $0.2\Omega_p$. In both case studied until now, it means, the electromagnetic EMIC and KA modes, the real frequency associated with the correspondent growth rate is peaked at frequency below the proton cyclotron frequency, characterizing a range of low frequency propagation.

High-frequency waves propagating in the auroral region as FMS, IW, EW and LH modes have been under consideration as well. For studying these modes, we have also used numerical programs, able to evaluate the dispersion relation for oblique plasma waves in a magnetic field, excited by parallel electron beams.

Applying initially the standard plasma conditions, we are able to observe the propagation and compare the growth rate results to the high-frequency modes. In both modes the real frequency associated with the correspondent growth rate peak, occurs above the proton cyclotron frequency.

We have also changed some plots from logarithmic to linear scale, in the sense of showing explicitly the negative imaginary frequency characterizing a damping predominance, since this imaginary part were totally absent in the picture shown by logarithmic scale.

The Figure 7 shows the FMS mode when θ = 89º. The growth decrease while k increases (λ decrease). Figure 8 shows the EW mode propagation when θ = 5º. It is also clear the absence of growth and the predominant presence of the wave damping. Figure 9 shows the plot ω, γ × θ to the IW mode for a fix k (k = 1000) and the angle θ varying between 1º and 89º. The wave growth increases when $\theta \to \pi / 2$.

Finally, we are going to show the LH modes because of different combinations among ω, γ, k and θ. First, we present in Figure 10 the mode by the plot ω, γ × θ for a fix k (k = 1000) and the angle θ varying between 1º and 89º. It is observed that the growth is predominant over the damping and decreases if θ increases. In the next Figures 11 and 12 the plots are still shown for a fix values of k (k = 500) and (k = 1500), respectively. Although, the growth is absent for any k below 500 and drops immediately above 1500 in the same background plasma conditions. In both cases, the growth is predominant over the range that include θ = 45º. Fixing in this angle, we plot the curve ω × k, shown by the Figure 13 and see the predominant growth in the range 500 <k< 1700. Out of this range, the damping is predominant, as it should be.

## IV. Cherenkov Damping

The numerical codes used in this paper is also able to calculate numerically the dielectric tensor elements, which are of paramount importance to obtain for each unstable mode the spectral energy, and momentum density and polarization. In order to show how it works, we calculate the anti-hermitian and hermitian parts of this tensor just for the LH mode, for θ = 45º, which is the angle where the LH mode grows faster (see Figures 10-13) for the auroral parameters used. In the Figures, 11-13 we saw very clear that the maximum spectral density (growth) occurred for k = 500.

The hermitian part also differs from the fluid model but collisionless dissipation is directly related to anti-hermitian part and the damping, γ, is given by de Assis and Tsui [1991].

The sequence of plots shows the hermitian and anti-hermitian tensor elements, corresponding to the Figure 13, what means, the plot that presents the larger growth. It is clearly seen from the hermitian plots, the terms $\varepsilon^H_{i\neq j} << \varepsilon^H_{i=j}$ whenever k ≈ 500, what means a distribution of energy between $E_\perp$ and $E_{//}$, as it should be since, θ = 45º. Being, however, larger $\varepsilon^H_{xx}$ and $\varepsilon^H_{zz}$.

It is also clearly seen from the anti-hermitian plots that the maximum growth occurs for k ≈ 500. This can be understood if one recalls equation [de Assis, 1991],

$$\frac{\gamma}{\omega} = \frac{\vec{E} \cdot \varepsilon^{AH} \cdot \vec{E}^*}{\vec{E} \cdot (\partial / \partial \omega)(\omega \varepsilon^H) \cdot \vec{E}^*} \qquad (6)$$

where $\vec{E}^*$ is the complex conjugate vector of $\vec{E}$.
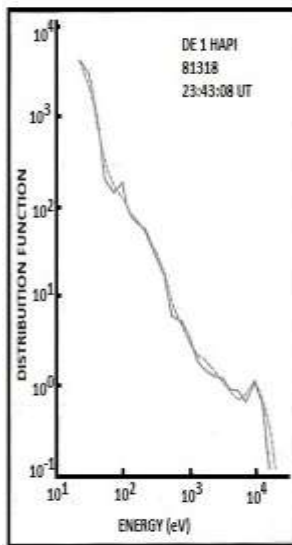
## Figures

Fig.1 – The picture shows an electron distribution function measured during an inverted-V structure represented by a solid line, while the dashed line represents a model function. (after Lin et al. 1989).
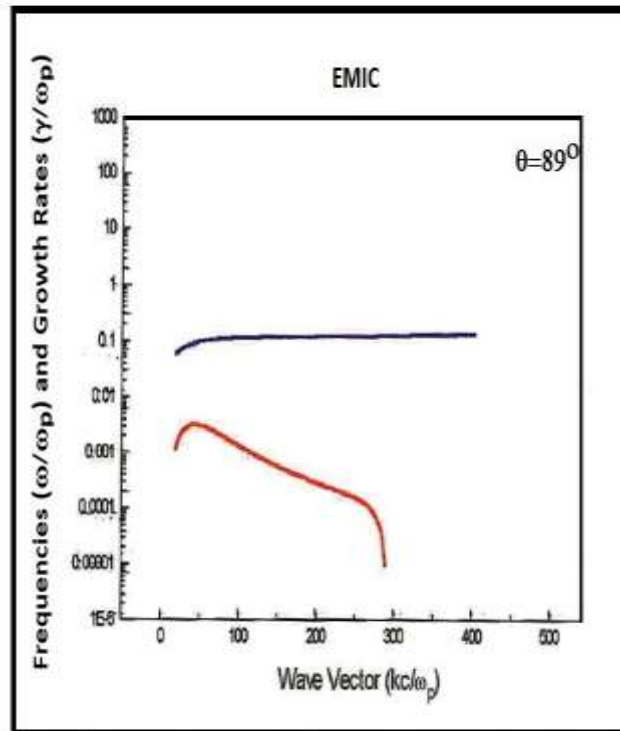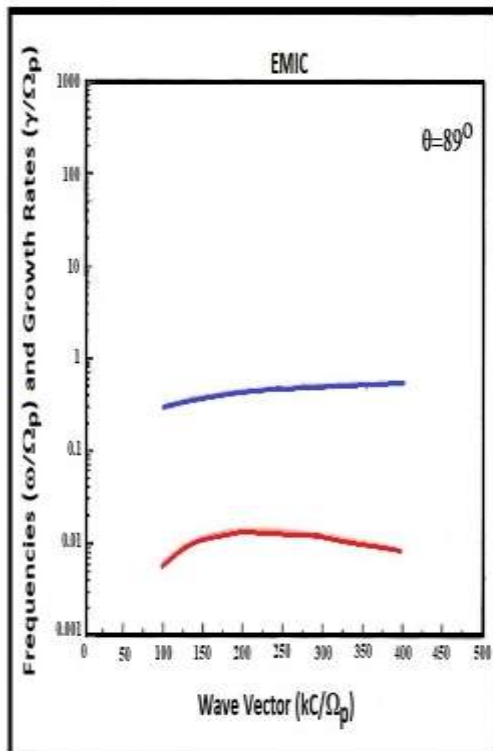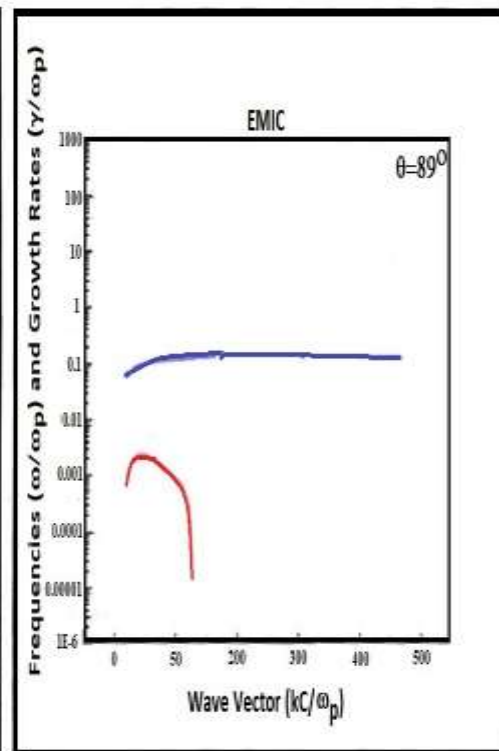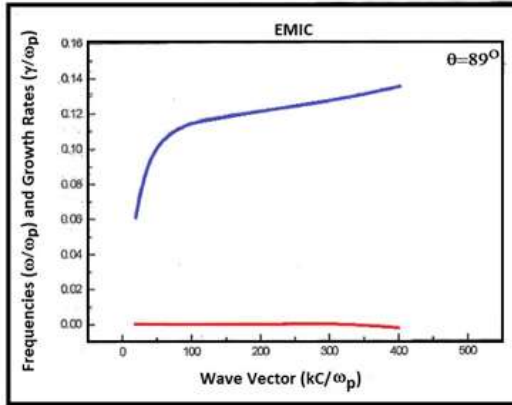


Fig. 2 - The real frequency, ω, (upper curve) and the growth rates, γ, (lower curve) of the EMIC wave for the inverted-V parameters given in the text. Both frequencies are normalized to ωp. The electron cyclotron frequency is 150 kHz. The hydrogen concentration is 90% and both, hydrogen and oxygen are suggested have the same temperature ($T_H = T_O = 15eV$). For all the components, $T_H / T_\perp = 1$.



Fig. 3 - The real frequency, ω, (upper curve) and the growth rates, γ, (lower curve) of the EMIC wave for the inverted-V parameters given in the text. Both frequencies are normalized to $\Omega_p$. The hydrogen concentration is 90% and both, hydrogen and oxygen are suggested have the same temperature ($T_H = T_O = 15eV$). For all the components, $T_H / T_\perp = 1$.



Fig. 4 - The real frequency, ω, (upper curve) and the growth rates, γ, (lower curve) of the EMIC wave for the inverted-V parameters given in the text. Hydrogen and oxygen are suggested have the same temperature ($T_H = T_O = 100eV$). Other parameters are the same as in Fig. 2

Fig. 5: The real frequency, $\omega$, (upper curve) and the growth rates, $\gamma$, (lower curve) of the EMIC wave for the inverted-V parameters given in the text. The rate between drift to the thermal velocity is 3. Other parameters are the same as in Fig. 2.
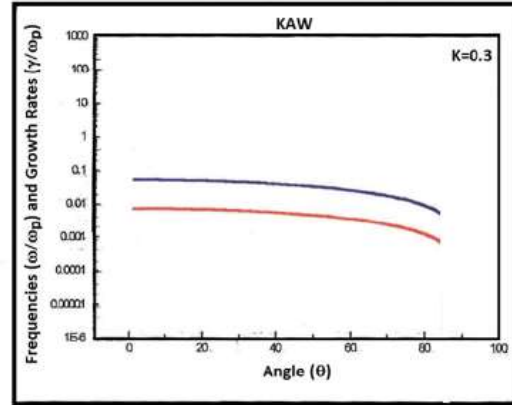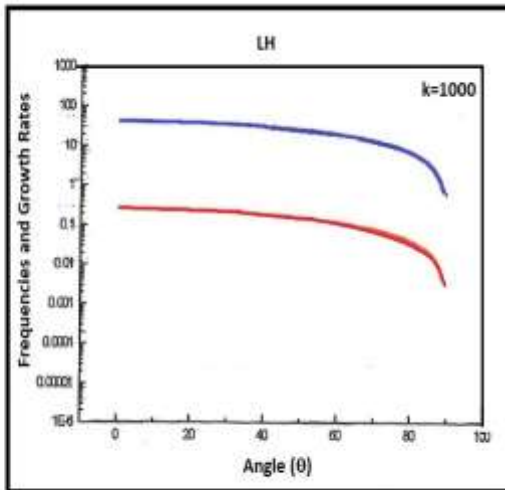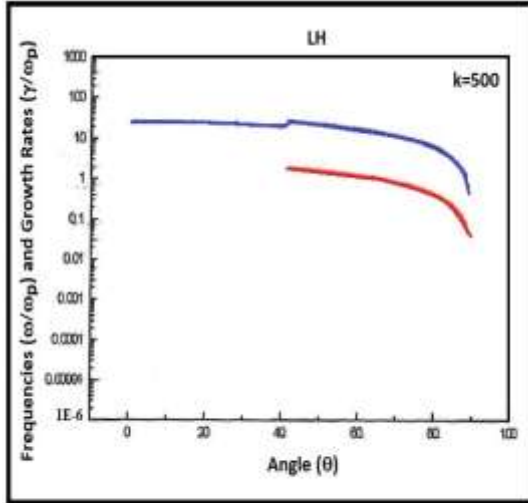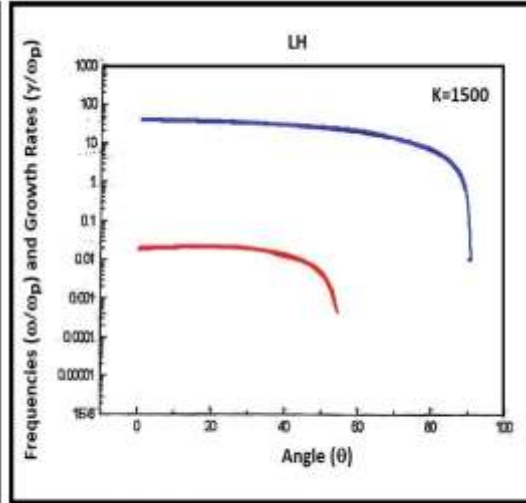


Fig. 6: The real frequency, $\omega$, (upper curve) and the growth rates, $\gamma$, (lower curve) of the KA wave. For these calculation k has a fix value (k = 0.3) and $\theta$ varies from $1^0$ to $89^0$.
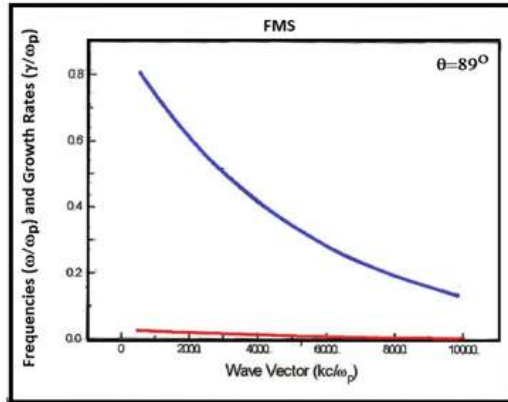


Fig. 7: The real frequency, $\omega$, (upper curve) and the growth rates, $\gamma$, (lower curve) of the FMS wave. Other parameters are the same as in Fig. 2.
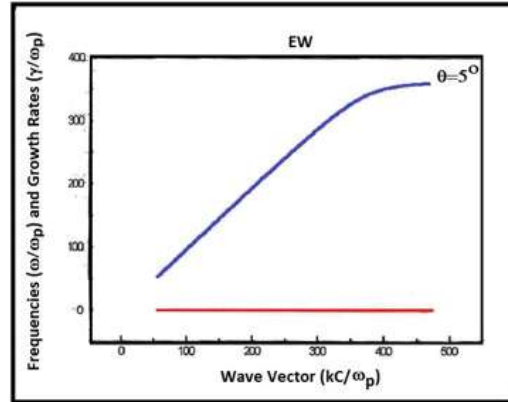


Fig. 8: The real frequency, $\omega$, (upper curve) and the growth rates, $\gamma$, (lower curve) of the EW wave. For these calculations the wave parallel angle is $\theta = 5^0$.
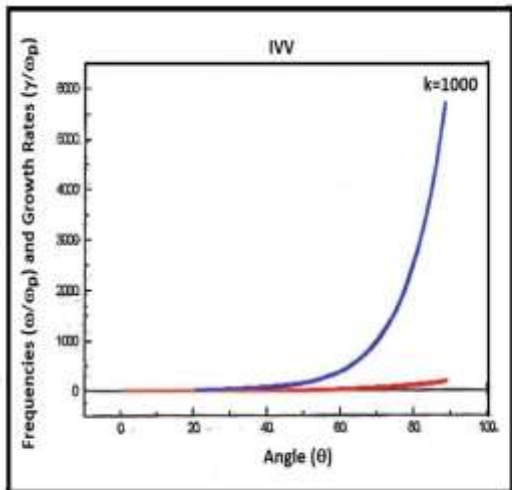


Fig. 9 - The real frequency, $\omega$, (upper curve) and the growth rates, $\gamma$, (lower curve) of the IVV wave. For these calculations, k has a fix value and $\theta$ varies from $1^0$ to $89^0$.



Fig. 10 - The real frequency, $\omega$, (upper curve) and the growth rates, $\gamma$, (lower curve) of the LH wave. For these calculation k has a fix value (k = 1000) and $\theta$ varies from $1^0$ to $89^0$.

Fig. 11 - The real frequency, ω, (upper curve) and the growth rates, γ, (lower curve) of the LH wave. For these calculations it has a fix value (k = 500) and θ varies from 1° to 89° as well as in Fig. 10.



Fig. 12 - The real frequency, ω, (upper curve) and the growth rates, γ, (lower curve) of the LH wave. For these calculations it has a fix value (k = 1500) and θ varies from 1° to 89° is now 30%. Other parameters are the same as in Fig. 10.
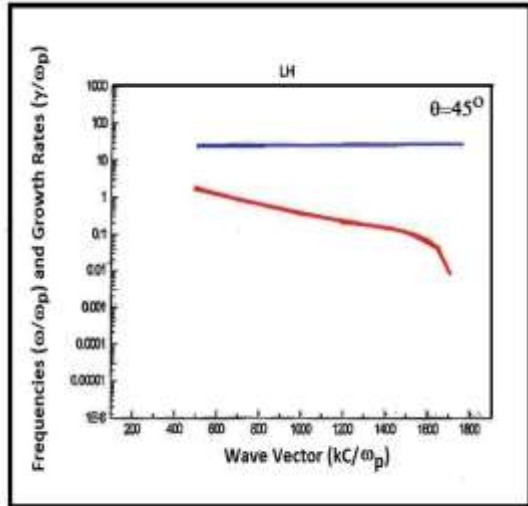


Fig. 13 - The real frequency, ω, (upper curve) and the growth rates, γ, (lower curve) of the LH wave. For these calculations the fix angle is 1° to 45°. Again, the beam density is 30%.
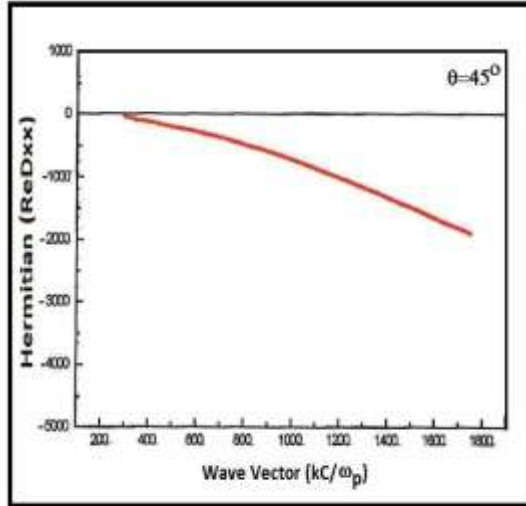


Fig. 14 - Plot of the hermitian part of the dielectric tensor element, showing the real element $D_{xx}$. All the hermitian and anti-hermitian plots below are related to the LH mode presented in the Fig. 13.
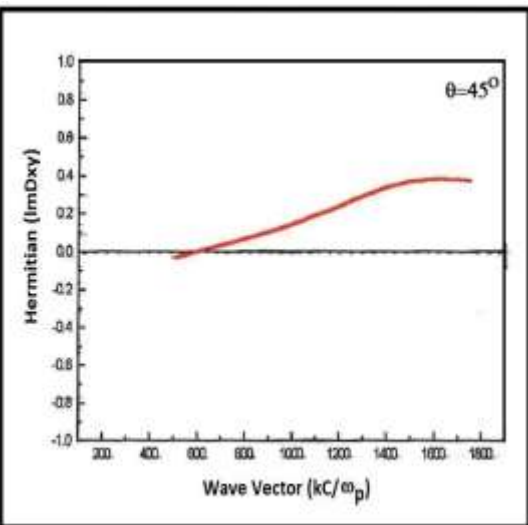


Fig. 15 - Plot of the hermitian part of the dielectric tensor element, showing the imaginary element $D_{xy}$.
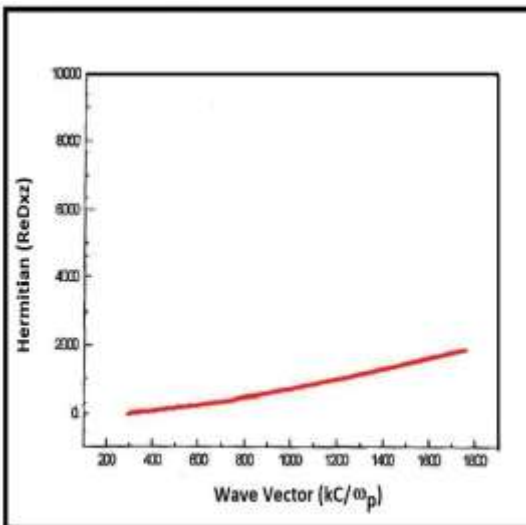


Fig. 16 - Plot of the hermitian part of the dielectric tensor element, showing the real element $D_{xz}$.
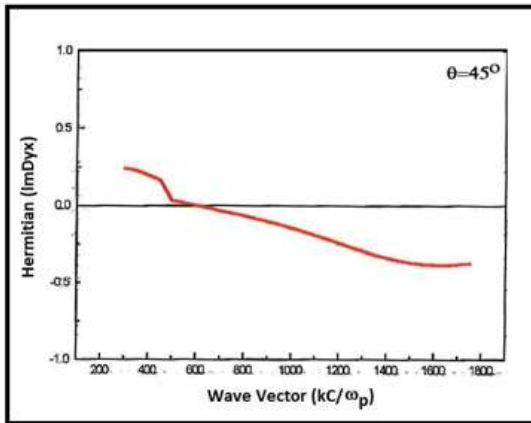
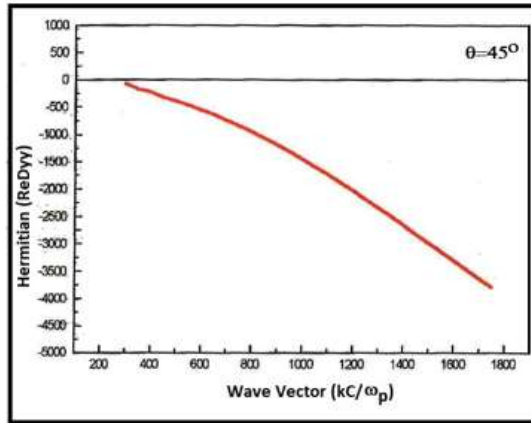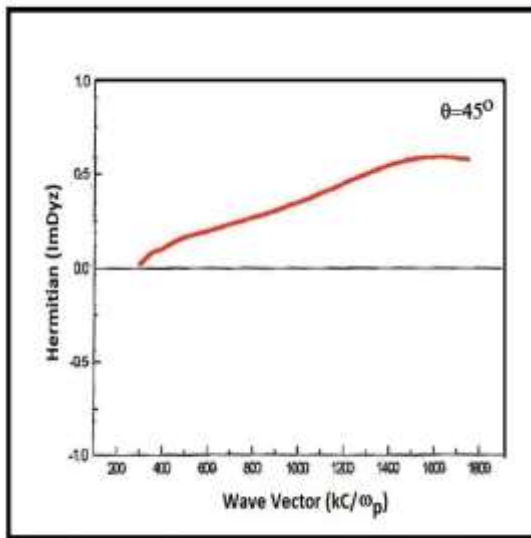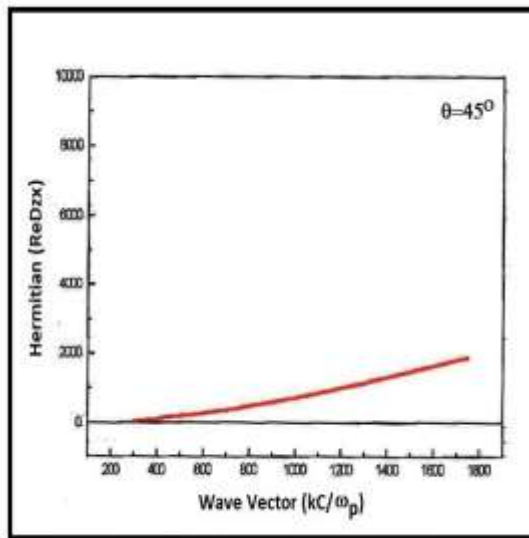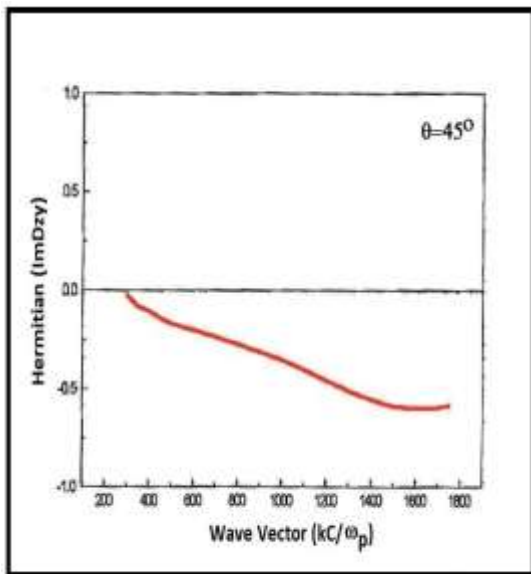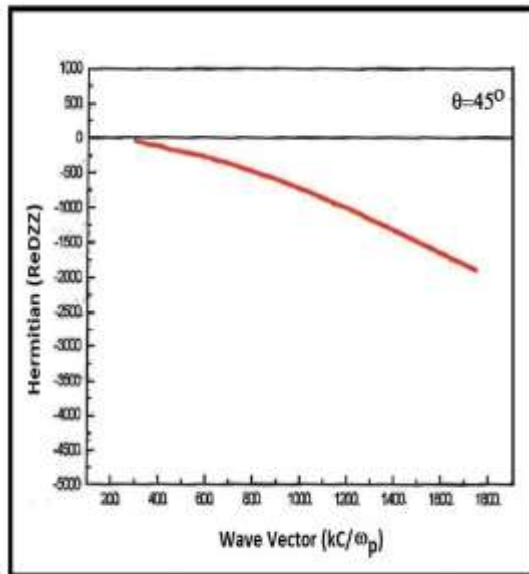Fig.17: Plot of the hermitian part of the dielectric tensor element, showing the imaginary element $D_{yx}$.



Fig. 18: Plot f the hermitian part of the dielectric tensor element, showing the real element $D_{yy}$.



Fig. 19 - Plot f the hermitian part of the dielectric tensor element, showing the imaginary element $D_{yz}$.



Fig. 20 - Plot of the hermitian part of the dielectric tensor element, showing the real element $D_{zx}$.



Fig. 21 - Plot of the hermitian part of the dielectric tensor element, showing the imaginary element $D_{zy}$.



Fig. 22 - Plot of the hermitian part of the dielectric tensor element, showing the real element $D_{zz}$.
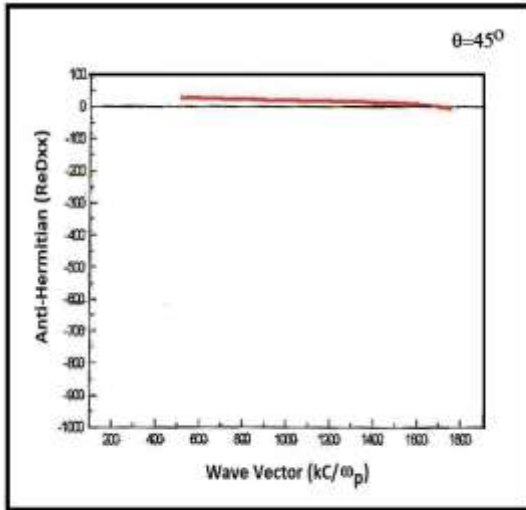
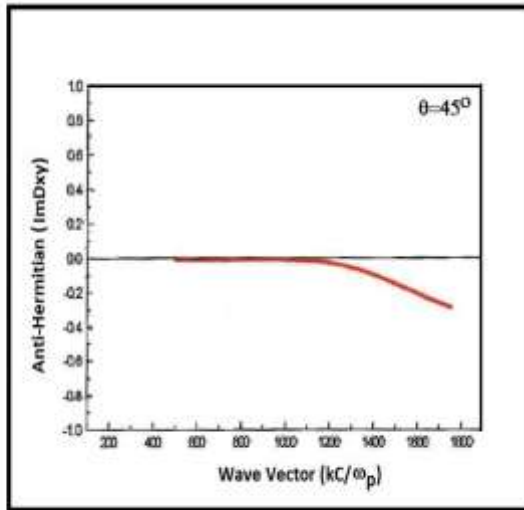Fig. 23 - Plot of the anti-hermitian part of the dielectric tensor element, showing the real element $D_{xx}$.



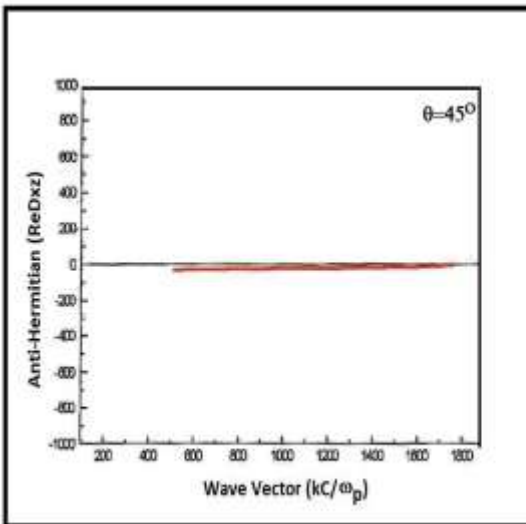Fig. 24 - Plot of the anti-hermitian part of the dielectric tensor element, showing the imaginary element $D_{xy}$.



Fig. 25 - Plot of the anti-hermitian part of the dielectric tensor element, showing the real element $D_{xz}$.
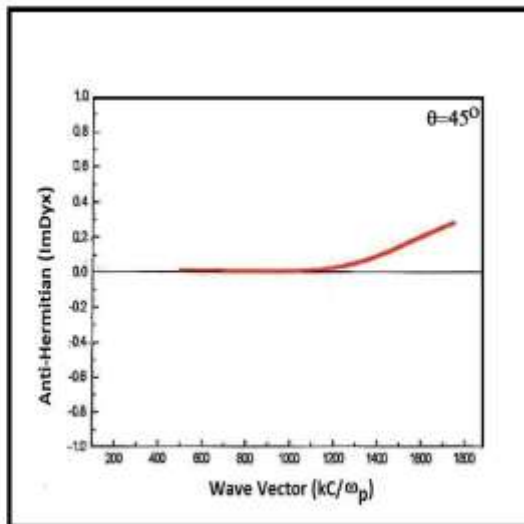


Fig. 26 - Plot of the anti-hermitian part of the dielectric tensor element, showing the imaginary element $D_{yx}$.



Fig. 27 - Plot of the anti-hermitian part of the dielectric tensor element, showing the real element $D_{yy}$.



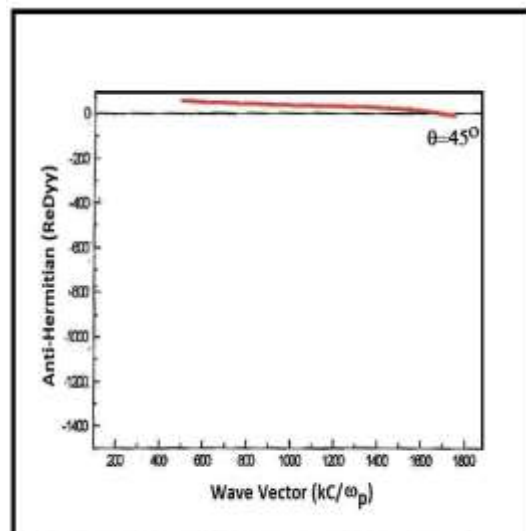Fig. 28 - Plot of the anti-hermitian part of the dielectric tensor element, showing the real element $D_{yz}$.

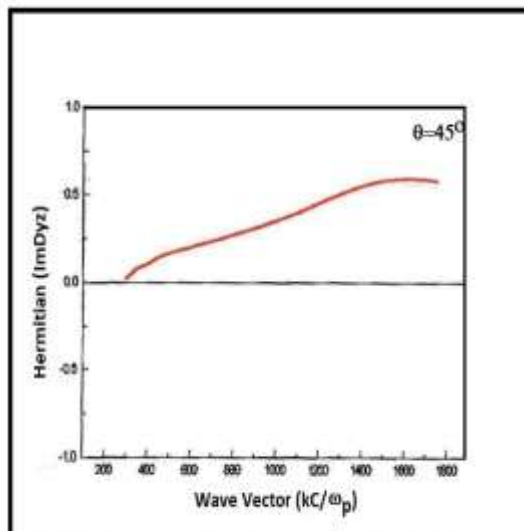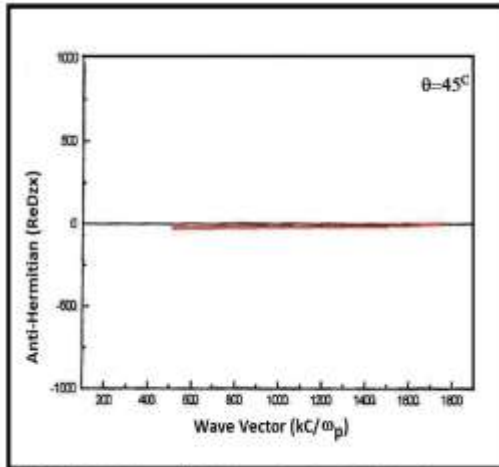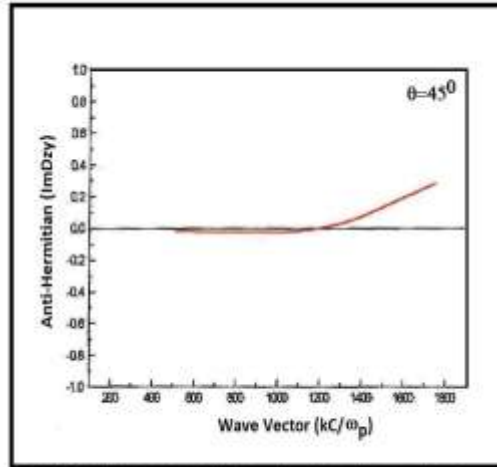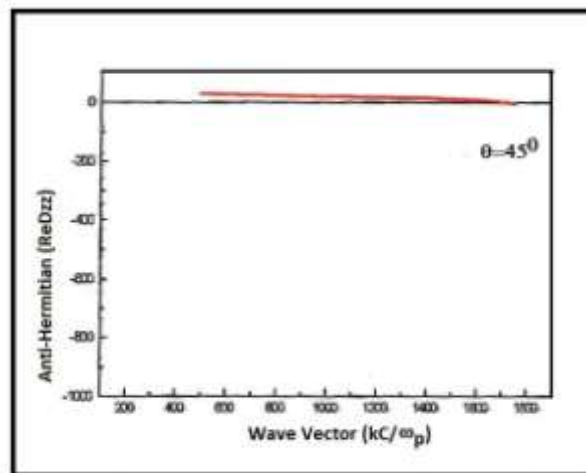Fig. 29 - Plot of the anti-hermitian part of the dielectric tensor element, showing the real element $D_{zx}$.



Fig. 30 - Plot of the anti-hermitian part of the dielectric tensor element, showing the imaginary element $D_{zy}$.



Fig. 31 - Plot of the anti-hermitian part of the dielectric tensor element, showing the real element $D_{zz}$.

# V. Discussion And Conclusions

The electron distribution functions measured by DE 1 satellite during its unusual auroral pass on day 318, 1981 [Winninghan and Burch, 1984], to conduct a linear instability analysis of low and high frequencies electromagnetic and electrostatic waves, have been used to investigate the presence of instabilities throughout the auroral region. Our purpose in analyzing these data has been to investigate the different modes, able to propagate whenever a source of free energy is available for generating as low as high-frequency waves, which can accelerate electrons and ions. Although, particle acceleration will not be treated here, but left as a topic of a next paper.

The background plasma parameters in our discussion are in agreement with Lin et al [1989]. Due the dynamic processes taking place in the bulk of the Earth environment, in particular auroral region, distinct phenomena may occur in response of these changes, not fully detected by the satellites. Waves in plasma is one of these phenomena affected directly by the dynamic processes, and our main interest is to investigate how waves can propagate under different plasma conditions. To do it, we have simulated numerically different changes in the plasma parameters in order to determine which modes can be excited and propagate in such conditions.

Our source of free energy is the energetic electron beam distribution in the inverted-V structures, detected during the inverted-V events [Figure 1]. Figures 2-5, show EMIC waves with frequency below the hydrogen cyclotron frequency at quasi perpendicular angles, under different plasma conditions simulated numerically. The background plasma has the same ions temperature of about 15 eV, but we have also considered in our analysis a 100 eV temperature just for comparison. Figure 4 shows the presence of instability for this temperature, where the growth rates is hardly affected, expanding in a narrow of wave number, while the real frequency is inconstant and fail in some ranges. The EMIC wave is still present even though the beam has a relativistic energy, as can be seen by the plot in the Figure 5.

Figure 6 and 7, still show the low-frequency modes differently from the EMIC waves. Figure 6 presents a plot which frequency varies with the angle for a fix wave number. This mode is denominated KA, its growth is relevant in a broad range, drops slowly when θ increases, but drops suddenly at θ = 87º. From the program output data, we observe that the polarization changed to right-hand at θ = 87º and turns again to left-hand after this point, suggesting some kind of linear mode conversion. As can be seen from the figure, the instability occurs over a narrow frequency band and the growth rate is peaked at $\omega / \Omega_p \sim 0.2$. In Figure 7, the plot shows the FMS wave for a fix angle θ = 89º. In this case, a weak turbulence can appear in the plasma due the small growth rate and a broad wave number spectrum.

We next discuss the presence of electromagnetic and electrostatic high-frequency instability in the same context presented above.

Figures 8 and 9 show respectively the electromagnetic EW and IW modes. The first mode propagate in a quasi-parallel direction at θ = 5º and presents a cutoff for $\omega \sim \Omega_e$. By the plot, it is easy to see the absence of the growth, characterizing a damping predominance. From the Figure 9, the growth is present but is very shy and the damping again is predominant. In both cases $\omega >> \Omega_i$ and the modes are recognized as high-frequency ones.

In the next plots are presented the electrostatic LH waves. The relevance of the this mode in our analysis take into account the facto f being a mode, which present the better growth rate from the same background plasma conditions.

Figures 10-12 show the presence of instabilities for three different fix wave numbers k = 100, 500 and 1500 respectively and θ varying from 1º to 89º. In the first figure, the growth is relevant for any angle, but decay slowly as the angle increases. From the second and third figures we can see that the presence of a growth common angle could be θ = 45º. Finally in Figure 13 the plot for this fix angle (θ = 45º) showing the predominant growth over a broad wave number band.

We conclude our analysis with the sequence of plots showing the hermitian and anti-hermitian parts of the tensor elements. The association with the spectral energy density can be found in Stix [1992]. The correspondent mode taken into account in this analysis was LH and the Figure 13 used since the growth is too expressive.

There are some important phenomena, which could be associated with the presence of instabilities inside the auroral region, for instance, ions heating and/or accelerations via wave-particle interaction. In the acceleration process, one of the most relevant aspect of the mode is the polarization, since an important requirement in this case should be resonance between wave and particles, and this is possible when the modes are left-hand polarized for the case of positive ions and right-hand polarized for the case of electrons. In the numerical code developed, we have the exact information about the wave polarization, for example, EMIC mode presents almost 100% left-hand polarization, while the IW mode almost 100% of right-hand polarization, along of their propagations through the auroral region. Another important information for charge particle acceleration that can be obtained from our plots is the spectral width, this quantity is important to study the acceleration using the quasilinear approach [de Assis et al., 1996].

With this code, we can also explorer other regions besides auroral region, and many other environment conditions that satellite investigation fail to cover the different aspects related with Strong variations because of dynamic processes taking place at different place and time.

## Acknowledgments

## References

[1]. de Assis, A. S. and K. H. Tsui, Coronal Loop Heating by Wave-Particle Interactions, The Astrophysical Journal, 366: 324-327, 1991.

[2]. de Assis, A. S., de Azevedo, C. A., C. Leubner, Electron Acceleration with Kinetic Alfvén Waves, PhysicaScripta T63, 241-243, 1996.

[3]. Lin, C. S., H. K. Wong, J. Koga, and J. L. Burch, Excitation of Low-Frequency Waves by Auroral Electron Beams, J. Geophys. Res., 94, 1327-1337, 1989.

[4]. Parks, G. K. 1991. Physics of Space Plasmas. USA: Addison-Wesley.

[5]. Persoon, A. M. , D. A. Gurnett, W. K. Peterson, J. H. Waite, Jr., J. L. Burch, and J. L. Green, electron density depletions in the night side auroral zone, J. Geophys. Res., 93, 1871, 1988.

[6]. Sharp, R. D., R. G. Johnson, and E. G. Shelley, Obervation of an ionospheric acceleration mechanism producing energetic (KeV) ions primarily normal to the geomagnetic field direction, J. Geophys. Res., 82, 3324, 1977.

[7]. Shelley, E. G., Johnson, and R. D. Sharp, Satellite observations of energetic heavy ions during a geomagnetic storm, J. Geophys. Res., 77, 6104, 1972.

[8]. T. H. Stix, 1992. Waves in Plasmas. American Institute of Physics.

[9]. Temerin, M., and R. L. Lysak, Electromagnetic ion cyclotron mode (ELF) waves generated by auroral electron precipitation, J. Geophys. Res., 89, 2849, 1984.

[10].    Wang et al. "nonlinear Kinetic Alfvén Wave with Poisson Equation Correction in the Low Aurora", Astrophysical and Space Science 240, 175-186, 1996.
[11].    Winningham, J. D., and J. L. Burch, Observations of large scale ion conic generation with DE 1, in Physics of Space Plasmas, SPI Conf. Proc. Reprint Sedr., vol. 5, edited by J. Belcher, H. Bridge, T. Chang, B. Coppi, and J. R. Jasperse, p.137, Scientific, Cambridge, Mass., 1984.
[12].    Yau, A. W. and Whalen, B. A., Ion Acceleration in the Low-and Mid-Altitude Auroral Ionosphere, Geophysical Monograph; 80/Robert Lysak, editor., 183-193, 1993.

Claudio Elias da Silva . "Excitation of Plasma Modes by Electron Beams." IOSR Journal of Applied Geology and Geophysics (IOSR-JAGG) , vol. 5, no. 5, 2017, pp. 31–43.